IEEE Access
Multidisciplinary ⋮ Rapid Review ⋮ Open Access Journal

Date of publication xxxx 00, 0000, date of current version 14 February, 2024.

Digital Object Identifier 10.1109/ACCESS.2023.1120000

Efficiency of cycled batteries analyzed through voltage-current phase differences

MARCUS T. WILSON[1], CHRISTOPHER J. DUNN[2], Vance Farrow[2], Michael J. Cree[2], (Senior Member, IEEE), and Jonathan B. Scott[2], (Life Member, IEEE)

[1]Te Aka Mātuatua – School of Science, University of Waikato, Private Bag 3105, Hamilton 3240, New Zealand (e-mail: marcus.wilson@waikato.ac.nz)
[2]School of Engineering, University of Waikato, Private Bag 3105, Hamilton 3240, New Zealand

Corresponding author: Marcus T. Wilson (e-mail: marcus.wilson@waikato.ac.nz).

ABSTRACT

Ageing of rechargeable batteries is routinely characterized in the frequency domain by electrochemical impedance spectroscopy, but the technique requires laboratory measurements to be made on a time scale of days. However, the normal cycling of a battery as it is used *in situ* provides equivalent information in the time domain, though extracting robust frequency information from a time series is challenging. In this work, we explore, in the time domain, the relationship between instantaneous voltage-current phase difference and cycle efficiency. Moreover, we demonstrate that phase measures can be used to identify battery ageing. We have cycled a 250 mA h Nickel-Cobalt cell several hundred times and used Hilbert Transforms to identify phase difference between voltage and current. This phase difference becomes closer to zero as the battery ages, commensurate with a drop in energy cycle efficiency. In another experiment, we applied a synthetic current profile mimicking behaviour of an electric car cell, to a 3.2 A h $LiNiMnCoO_2$ cell, for $\sim$100 days. For this more complicated profile with a wide range of frequency content, we used wavelet analysis to identify changes in phase difference and impedance as the battery aged. For this cell, drop in cycle efficiency was associated with a rise in internal resistance. The results imply that time-series analysis of *in situ* measurements of voltage and current, when applied with equivalent circuit models and underlying theory, can identify markers of battery ageing.

INDEX TERMS Battery, Constant Phase Element, Efficiency, Fractional Capacitance, Time-series analysis

I. INTRODUCTION

BATTERY state of health (SoH) is a loose term generally used to describe of the performance of a battery when compared to an equivalent 'new' battery [1]. State of Health can manifest itself in various ways, such as charge or energy capacity, energy cycle efficiency and ability to deliver power, and can be estimated in numerous ways in practical applications [2]. Degradation is associated with many different failure mechanisms [3], [4] and can show itself through many ways, such as increased charge transfer and diffusion resistance, reduced current density, decreased voltage, and heat generation [5]. Frequently, battery ageing is clearly demonstrated through changes in impedance spectrum [6]–[9] but electrochemical impedance spectroscopy (EIS) often requires long measurement times in the laboratory, and thus is impractical for many battery applications, although in some cases more rapid measurements are possible [10].

Equivalent circuit models, using an array of capacitors, resistors, and constant phase elements (CPEs), have been well used to describe batteries [11]–[13]. Variations in different circuit elements will lead to variations in energy cycle efficiency, charge capacity, *etc.*, and it is attractive to seek to describe ageing of batteries in terms of these elements. Indeed, Farrow has used measurements of impedance spectrum to show a change in circuit elements as ageing occurs [8], and Mauracher & Karden have used electrochemical impedance spectroscopy to model changes in lead-acid batteries [14]. Significantly, combining EIS with time domain measurements, Messing *et al.* have identified changes in circuit elements with ageing from relaxation effects [15].

In this work we demonstrate that a change in order of a constant phase element in an equivalent circuit influences cycle energy capacity, via a change of phase between the voltage and current. Changes in phase have been previously recognized as underlying signals for SoH of lithium-ion batteries [2]. Importantly the phase changes can be extracted

from time-series data acquired while the battery is cycled. We first relate phase and energy efficiency for a CPE, through a theoretical analysis, as shown in Sec. II. We demonstrate that, for a CPE, we expect a relationship between cycle energy efficiency and phase between V and I. We then, in Sec. III, describe and analyze with Hilbert transforms and wavelet analysis the results of three experiments, using different batteries and charging-discharging cycles, that elucidate the relationship between phase and cycle efficiency. We demonstrate that for one of these experiments, changes in efficiency as the battery ages are related to phase changes. However, for another experiment, they are related to an increase in resistance. Finally, in Sec. IV, we put these results into the context of equivalent circuit models and suggest how time-series analysis of voltage and current can be used to elucidate changes in SoH.

II. THEORY

A. CONSTANT PHASE ELEMENTS

A constant phase element (CPE) or fractional capacitor can be defined through the fractional derivative relationship between current I and voltage V:

$$I(t) = C_f \frac{d^\alpha V}{dt^\alpha}, \tag{1}$$

where t is time, C_f is the fractional capacitance, and d^α/dt^α denotes the fractional derivative of order α, where $0 < \alpha < 1$. Fractional calculus has a secure mathematical base [16] including for application to batteries [17]. For the purposes of this work, the relationship is best discussed in terms of a response to a sine wave stimulus. For a sine wave current input, the voltage responds as a sine wave, but with a phase difference determined by the fractional order α. Specifically, constructing the impedance as the complex voltage (amplitude and phase) divided by the complex current, we have:

$$Z(\omega) = \frac{1}{C_f (j\omega)^\alpha} \tag{2}$$

where ω is the angular frequency ($= 2\pi f$ where f is the frequency) and $j^2 = -1$. Of importance is the phase (argument of Z), which is $\arg(j^{-\alpha}) = -\pi\alpha/2$. This phase is independent of frequency, hence the term 'constant phase element'. In the limit of $\alpha \to 1$ the CPE behaves as a capacitor; in the limit of $\alpha \to 0$ the CPE behaves as resistor. The special case of $\alpha = 0.5$ describes a Warburg element, commonly used in modelling of electrochemical processes, for example with the Randles circuit [18].

CPEs have been commonly used in models of batteries. For example, the model of Westerhoff *et al.* which explicitly considers the physical behaviour of the various structures of a battery, contains three CPE elements in addition to two Warburg elements, two capacitors and nine resistors [12]. Westerhoff's model associates electronic components with physical processes. However, for practical purposes, many fewer elements are needed to describe a battery [13], [19], with Poihipi *et al.* using just two CPEs and a resistor to effectively model experimental results [11]. Such a reduced phenomenological model makes attribution of changes in electronic component values to particular chemical and physical processes difficult. Indeed, experimental measurements of impedance [8], [20]–[22] suggest that in many cases simply a single CPE may be sufficient in series with a resistor might be a sufficient equivalent circuit to describe a battery.

B. ENERGY EFFICIENCY OF CPE

For a rechargeable battery, the energy efficiency of a cycle, ϵ, defined as the energy taken out of the battery during a discharge divided by the energy put in during a charge, is of significance. For a pure capacitor ($\alpha = 1$) there is no energy loss and $\epsilon = 1$; in contrast for a pure resistor ($\alpha = 0$) there is no energy stored and $\epsilon = 0$. In general, the efficiency of a battery cycle will depend on the shape of the cycle. In some special cases, it is possible to derive the efficiency mathematically.

The case of a single rectangular charge and discharge pulse (where charging and discharging currents are both constant, but not necessarily equal) has been analyzed by Hartley *et al.* [23], [24]. By setting the charge and discharge currents and times to maximize energy efficiency, one obtains an efficiency directly related to the fractional order α:

$$\epsilon = (2^\alpha - 1)^2 . \tag{3}$$

While efficiency is dependent on α, the actual values of energy into the battery during the charge and the energy taken out of the battery during the discharge, depend on the currents and cycle times.

A second case in which we can explicitly derive the efficiency of a CPE is that of a continuous sine wave input. In the analysis below, we derive the efficiency under a sine wave stimulus for the case of a CPE in series with a resistor (denoted CPE-R), which is a reasonable circuit model for many batteries [8], [11]. A CPE-R model has a knee angular frequency defined where $|Z(\omega)| = R$; below this angular frequency the CPE dominates the impedance. We use the standard convention for batteries that *positive* and *negative* currents correspond to *charging* and *discharging* of the battery respectively. For the case of a sine wave current,

$$I(t) = I_0 \sin(\omega t), \tag{4}$$

the voltage across the CPE, assuming there is a constant starting voltage offset V_0 as a result of charging a CPE a long time in the past, responds as:

$$V_{CPE}(t) = V_0 + V_a \sin(\omega t + \theta) \tag{5}$$

where $V_a = |Z(\omega)| I_0$ is the amplitude of the a.c. part of the waveform, and $\theta = -\alpha\pi/2$ is the phase, *i.e.* the voltage trails the current by $\alpha\pi/2$. Note that V_a depends on frequency through $|Z|$. The voltage across the resistor, R, is simply IR, and thus the total voltage over the CPE-R elements is

$$V(t) = V_0 + V_a \sin(\omega t + \theta) + I_0 R \sin(\omega t). \tag{6}$$

We assume that $V(t)$ is always positive. For rechargeable batteries in normal operation, this will always be the case. Then the sign of the instantaneous power, $P(t) = V(t)I(t)$, is determined by the sign of the current $I(t)$, positive in the first half-cycle and negative in the second. The energy into the CPE-R circuit in the first half-cycle is given by:

$$E_{in} = \int_{t=0}^{T/2} V(t)I(t)dt. \tag{7}$$

Writing out $V(t)$ and $I(t)$ explicitly leads to

$$E_{in} = \int_{t=0}^{T/2} V_0 I_0 \sin(\omega t)dt + \int_{t=0}^{T/2} V_a I_0 \sin(\omega t)\sin(\omega t+\theta)dt + \int_{t=0}^{T/2} I_0^2 R \sin^2(\omega t)dt \tag{8}$$

where T is the period of the sine wave. Performing the integrals yields

$$E_{in} = \frac{V_0 I_0 T}{\pi} + \frac{V_a I_0 T\cos\theta}{4} + \frac{I_0^2 RT}{4}. \tag{9}$$

The energy put *into* the CPE in the *second* half-cycle is given by:

$$E_{in}^{(2)} = \int_{t=T/2}^{T} V(t)I(t)dt \tag{10}$$

which is

$$E_{in}^{(2)} = \int_{t=T/2}^{T} [V_0 + V_a\sin(\omega t+\theta) + I_0 R\sin(\omega t)]\, I_0\sin(\omega t)dt. \tag{11}$$

The quantity $E_{in}^{(2)}$ is *negative*, since $I(t)$ is negative during the second half-cycle. We can perform the integration to give:

$$E_{in}^{(2)} = -\frac{V_0 I_0 T}{\pi} + \frac{V_a I_0 T\cos\theta}{4} + \frac{I_0^2 RT}{4}. \tag{12}$$

The energy taken *out* of the CPE in the second half-cycle, is the negative of the energy put in, that is $E_{out} = -E_{in}^{(2)}$.

Thus we can define the efficiency as being $\epsilon = E_{out}/E_{in}$ which is:

$$\epsilon = \frac{V_0 I_0 T/\pi - V_a I_0 T\cos\theta/4 - I_0^2 RT/4}{V_0 I_0 T/\pi + V_a I_0 T\cos\theta/4 + I_0^2 RT/4}. \tag{13}$$

Multiplying numerator and denominator by $\pi/V_0 I_0 T$, and writing the voltage over the resistor as $V_r = I_0 R$ gives:

$$\epsilon = \frac{1 - \pi V_a\cos\theta/4V_0 - \pi V_r/4V_0}{1 + \pi V_a\cos\theta/4V_0 + \pi V_r/4V_0}. \tag{14}$$

In the limit of $\alpha \to 1$, and $R \to 0$, in other words the CPE-R equivalent circuit of the battery becoming a pure capacitor, $\cos\theta \to 0$ and $V_r \to 0$, and thus $\epsilon \to 1$ as we expect.

C. APPLYING EFFICIENCY MEASURES TO REALISTIC SITUATIONS

We emphasize that Eq. (14) applies to a sine wave current stimulus delivered to a single CPE in series with a resistor. In the limit of small currents (long charge/discharge times) any resistive effects will become small. For example, if the battery were described by a CPE in series with a resistor, the energy dissipated over the resistor would become negligible as the charge/discharge currents were reduced. Therefore, as one reduces the charge/discharge current, the final term in the numerator and denominator of Eq. (14) will become negligible.

In practice, the current can be far from sinusoidal. A realistic waveform will consist of non-harmonic periods of charge and discharge, over a range of different frequency scales. We note however that Eq. (14) gives a value of ϵ that is *independent of frequency* and depends only on (a) the phase angle $\theta = \pi\alpha/2$ and (b) the ratio of the amplitude of the voltage variation over the CPE, V_a, to the constant offset term V_0, and, if the current is large enough, (c) the ratio of the amplitude of the voltage over the resistor, V_r, to the constant offset term V_0. It is therefore reasonable to hypothesize that efficiency in realistic (non-sinusoidal) situations will depend most significantly on these dimensionless terms. In typical situations cycling of a battery is performed between prescribed voltage limits and thus V_a and V_0 will be defined independently of charging rate.

If the ratio of V_a to V_0 is rather less than one (which practically would likely be the case, *e.g.* for a battery cycled between 2.9 V and 3.3 V one can attribute V_0 = 3.1 V and V_a as 0.2 V), and the current is small so that V_r/V_0 is negligible, the binomial theorem approximates Equation (14) as:

$$\epsilon \approx 1 - \frac{\pi V_a\cos\theta}{2V_0}. \tag{15}$$

We note here that V_a is the amplitude of the assumed sine-wave and V_0 the mean voltage. We emphasize that Eq. (15) applies rigorously only for the case of a low-current sine wave stimulus, but rigorous generalization for more complicated waveforms is mathematically challenging. Nevertheless, the analysis demonstrates a relationship between cycle energy efficiency and phase differences — thus we expect in a general case a loss of cycle energy efficiency, for example due to ageing, to be accompanied by a changes in phase between V and I where the battery can be described as a CPE. Note however that if resistance R is significant, which will be the case at the higher frequencies, changes in cycle efficiency could also be attributed to changes in R.

III. EXPERIMENTAL METHODS AND ANALYSIS

We have carried out three separate experiments in order to demonstrate and confirm the relationship between efficiency to the fractional order, including in realistic battery operating conditions.

In the first experiment, we have cycled a battery using rectangular current pulses, at ever-decreasing currents. In the

limit of zero current one would expect the effect of any series resistance to disappear, and we would be left with the behaviour of the CPE. Specifically, we expect that a plot of current and voltage would show hysteresis and the energy efficiency would be related to α. We confirm this is the case.

In the second experiment, we have cycled a battery over several weeks in an attempt to wear it out, using some standardized charge-discharge cycles. We extract the energy efficiency over each cycle and show it is related to the phase difference between the voltage and current signals. In particular, as the battery ages, the energy efficiency drops while the phase between voltage and current moves towards zero in the manner expected.

Finally, we have cycled another battery over several weeks with a current profile more akin to what would be expected for an electric vehicle (EV), consisting of a time of rapidly-changing, mostly negative currents (corresponding to the EV being in use), followed by a time of zero current (corresponding to the EV being parked), and then a time of constant positive current (corresponding to charging), repeated over many days with small variations. We have extracted ϵ for these cycles, and have used the Multiscale Oscillatory Dynamics Analysis (MODA) toolbox of Lancaster University [25], [26], available at github.com/luphysics/moda to identify the phase relationship between voltage and current. All experiments were performed in an air-conditioned room where ambient temperature was kept between 21.0–22.5°C. Raw data is available from the authors on request.

A. LOW FREQUENCY CYCLING

1) Experimental method

In the first experiment we cycled a 4.8 A h, 3.7 V, $LiNiCoAlO_2$ (NCA) 21650 cell using a constant-current charge followed by a constant-current discharge using the same current as for the charge. Specifically, for a given current, we cycled the battery several times between lower and upper voltage limits of 3.0 V and 4.3 V respectively. We used currents of 5 A, 2 A, 1 A, 0.5 A, 0.2 A, 0.1 A and 0.05 A in that order, recording voltage and current as a function of time. We have evaluated the energy in and energy out for each of the cycles using Eqs. (7) and (10) respectively, and thus found the efficiency. From the efficiency in the low current limit we estimate α using Eq. (15) and compare the result to a value of α measured from an impedance spectrum obtained using the method of Dunn *et al.* [9], [20].

2) Results

Figure 1 shows a plot of voltage against charge for the various charge-discharge currents. At the lowest currents hysteresis remains, indicating that there is energy loss. The voltage against charge plot is roughly linear over much of the voltage range, although it shows some regular fluctuation particularly at the higher voltages and a rapid increase in gradient at both ends of the voltage range. We ignore these tails in our processing, and identify a voltage range here of 3.4 V to 4.2 V for the linear portion. We also note that the charge capacity of the cell increases as current decreases, consistent with a fractional element being involved [27].

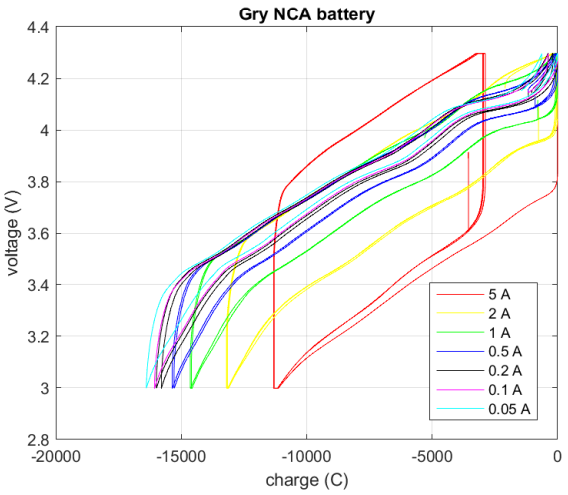

FIGURE 1. A plot showing hysteresis in the NCA battery at various constant charge-discharge currents. The currents used are given in the legend. Adapted from [27].

TABLE 1. The energy in and out of the battery, E_{in} and E_{out} respectively, and the cycle efficiency ϵ, at different charge-discharge currents during the battery cycling of Fig. 1.

Current (A)	E_{in} (kJ)	E_{out} (kJ)	ϵ
5	34.14	28.54	0.836
2	51.86	47.64	0.919
1	57.10	54.39	0.953
0.5	58.97	57.40	0.973
0.2	60.77	60.04	0.988
0.1	61.78	61.04	0.988
0.05	62.89	62.13	0.988

3) Analysis

The energy in and out of the cell during the charge and discharge half-cycles, found by integrating $V(t)I(t)$ over time, are shown in Table 1. In the limit of zero current, the efficiency approaches 0.988; this is close to 1 indicating that the cell is very like a capacitor but is clearly less than 1 showing that loss mechanisms are present. Applying Eq. (15) with voltage limits of 3.4 V and 4.2 V (thus $V_0 = 3.8$ V and $V_a = 0.4$ V) with a measured efficiency of 0.988 gives us $\theta = 1.497$ rad $= 85.8°$, and hence $\alpha = 0.954$.

We can verify the value for the fractional order α from the impedance spectrum. Figure 2 shows a plot of the of the impedance of the cell against frequency, on logarithmic axes, as (a) magnitude and (b) phase. Fitting a straight line to the lowest seven frequency points of (a) yields a gradient of $-0.976(8)$ and hence we infer a value of α from the impedance measurement of 0.976(8), larger but close to that estimated through the efficiency.

In the limit of zero current, we expect that any resistive loss becomes negligible. By attributing the energy loss to a CPE, we have estimated an order for the CPE of 0.954. This is slightly lower than that found by measuring an impedance

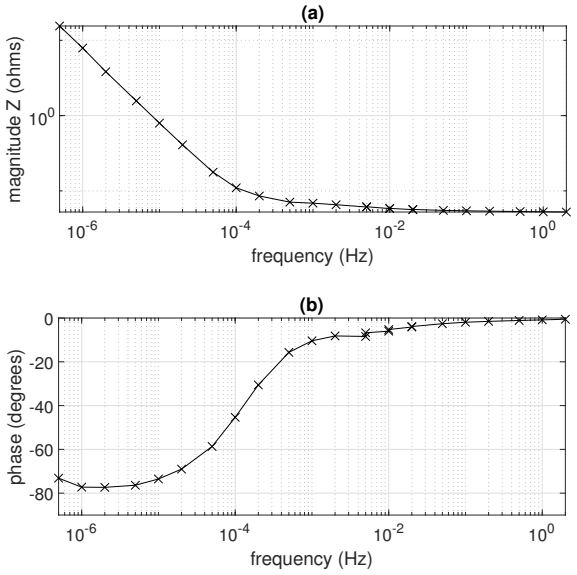

FIGURE 2. The impedance spectrum of the NCA battery, presented as (a) magnitude and (b) phase.

spectrum.

We note that we have estimated the order of the CPE, α, using Eq. (15) which strictly only applies to a CPE-R model driven by a sine-wave stimulus, in the limit of low currents. The experimental cycling has been carried out, for practical reasons, with a rectangular stimulus and so the calculated value of α should be seen as an estimate only. Nevertheless, it is encouraging that the value estimated from energy efficiency and the value from the impedance spectrum, two very different methods, are roughly in agreement.

B. STEREOTYPED CYCLES

The second experiment consists of ageing a battery by performing repetitive charge-discharge cycles. The cycle efficiency is monitored and related to phase difference between voltage and current. A repetitive but non-sinusoidal cycle can be analyzed using Hilbert Transforms in order to extract the phase difference between voltage and current. For example, Hilbert Transforms have been used in the context of batteries to validate electrochemical impedance spectrum measurements [28] and to detect disturbances in power systems via phase changes [29].

1) Experimental method

A 250 mA h INR Nickel-Cobalt cell was cycled in the laboratory using sets of 30 charge-discharge cycles, each of a particular form of constant-current-constant-voltage (CC-CV) cycling. In CC-CV, a constant charging current I_{ch} is applied to bring the voltage to a specified upper voltage $V_{\rm h}$. Then the battery is held at this voltage by reducing the current, until the current decays to a specified lower value I_{low}. The battery is then discharged with a constant discharge current

TABLE 2. The different cycle types used, defined in terms of the charge current I_{ch}, discharge current I_{dis}, upper voltage $V_{\rm h}$, lower voltage $V_{\rm l}$, lower bound on charging current during the constant voltage phase I_{low}, and time spent at zero current t_0.

Type	I_{ch} (A)	$I_{\rm dis}$ (A)	$V_{\rm h}$ (V)	$V_{\rm l}$ (V)	I_{low} (A)	t_0 (s)
Cyc	0.16	-0.16	4.3	3.3	0.03	600
Shal	0.16	-0.16	4.0	3.3	0.03	600
Float	0.16	-0.16	4.3	3.3	0.003	600
Asym	0.04	-0.16	4.3	3.3	0.01	600
Mysa	0.16	-0.04	4.3	3.3	0.03	600
Slow	0.08	-0.08	4.3	3.3	0.03	600

TABLE 3. The sequence of CC-CV cycling, in sets of 30 cycles.

Sequence	Cycle set	Cycle type	Cumulative cycles
1	1	Cyc	310
2		Shal	340
3		Float	370
4	2	Cyc	400
		Impedance measurement	
5	3	Cyc	430
6		Asym	460
7		Mysa	490
8	4	Cyc	520
		Impedance measurement	
9		Slow	550
10	5	Cyc	580
11		Shal	610
12		Float	640
13		Slow	670
14		Asym	700
15		Mysa	730
16	6	Cyc	760

$I_{\rm dis}$, until its voltage reaches a specified lower bound $V_{\rm l}$. Then a period of zero current is applied for a defined time period t_0. The cycle is then repeated. Six different variations of the CC-CV cycling were used, as outlined in Table. 2 and applied in the sequence shown in Table. 3. The forms of cycle differed in terms of maximum and minimum voltage, charge and discharge currents, and the lower current bound to end the constant voltage phase. A standard cycle, denoted here by 'Cyc' was returned to several times in order to allow a direct evaluation of ageing effects. The current characteristics of a standard cycle, along with a voltage response, are shown in Fig. 3. Before this experiment, the cell had already been cycled approximately 280 times in various ways. At two points in the experiment the cycling was interrupted to perform a measurement of impedance on the cell [9]. The experiment took nine weeks total duration.

We discarded the first three cycles of each set of 30 cycles to allow the voltage signals to stabilize. Cycle efficiency ϵ was evaluated for each cycle, and averaged over the remaining 27 cycles in each set. We also, for the time period spanned by the final 27 cycles, calculated the Hilbert Transforms of current and voltage using Matlab. The phase $\phi_I(t)$ of the current waveform was then extracted as:

$$\phi_I[I(t)](t) = \tan^{-1}\left(\frac{H[I(t)](t)}{I(t)}\right), \qquad (16)$$

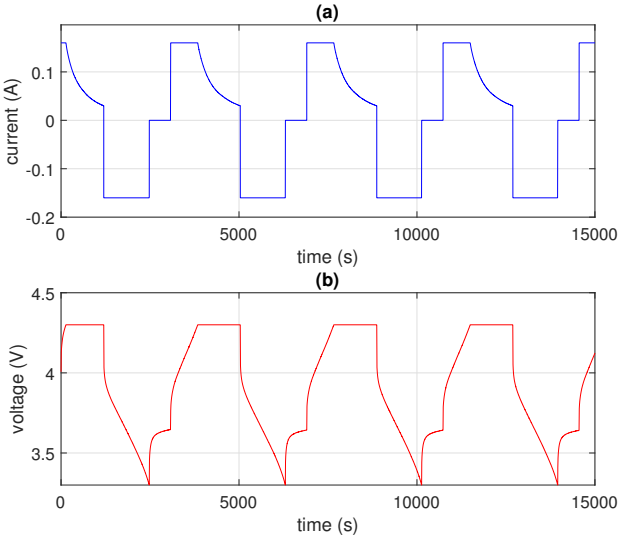

FIGURE 3. The current (top, blue) and voltage response (bottom, red) for a few standard 'Cyc' cycles.

where $H[I(t)](t)$ denotes the Hilbert transform of $I(t)$ and the inverse tangent is evaluated using the signs of the numerator and denominator using the 'atan2' function in order to be continuous from $-\pi$ to π. The phase $\phi_V(t)$ was similarly extracted for the voltage waveform $V(t)$. The phase angle $\phi(t) = \phi_V(t) - \phi_I(t)$ was found, representing an instantaneous phase difference between $V(t)$ and $I(t)$. The mean phase difference over the final 27 cycles of each 'Cyc' set was calculated.

2) Results

In Fig. 4(a) we show, for each of the six sets of 30 'Cyc' cycles, the mean energy into the cell during the charge periods (averaged across the final 27 cycles), and the mean energy out of the cell during the discharge periods (similarly averaged over the final 27 cycles). In Fig. 4(b) we show the distribution of cycle efficiencies for the six 'Cyc' sets.

Figure 5 shows the distribution of phase differences between V and I over each of the six 'Cyc' sets, as found through the Hilbert transform. The second and subsequent sets are displaced downwards by 0.1 on the y-axis for clarity. It is immediately evident that the phase distribution moves towards zero as the battery ages.

3) Analysis

Figures 4 and 5 show that as the battery ages, (i) the cycle efficiency drops and (ii) the distribution of phase differences becomes less negative. These changes are summarized in Table. 4. Furthermore, we have used Eq. (15) with $V_0 = 3.8$ V and $V_a = 0.5$ V, in order to estimate the phase angle θ from the measured efficiencies; these are shown in Tab. 4 as θ_{est}. These can be compared with the mean measured phase differences as found via the Hilbert transforms, indicated as θ_{H}.

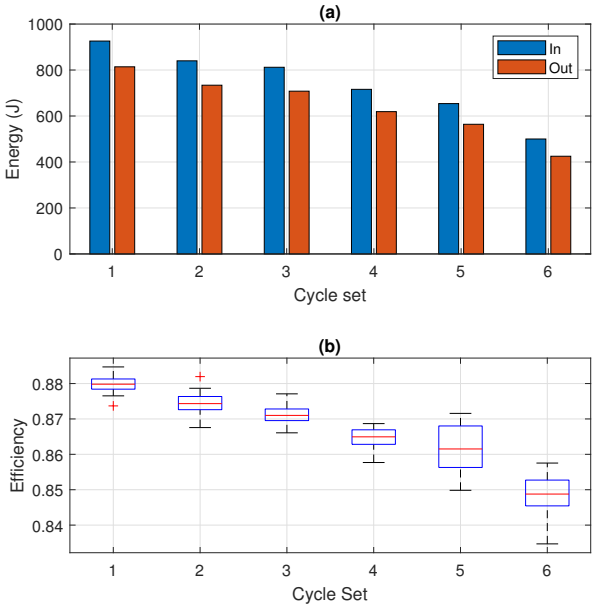

FIGURE 4. (a) The mean energy in and out of the battery during each of the six sets of standard cycles (excluding the first 3 cycles in each set). (b) The distribution of the cycle efficiencies for each set. The red line shows the median; the boxes show lower quartile and upper quartile; the extending lines showing the range of the data. Outliers are marked with red crosses. Note how ***both*** the energy capacity and the efficiency drop with age.

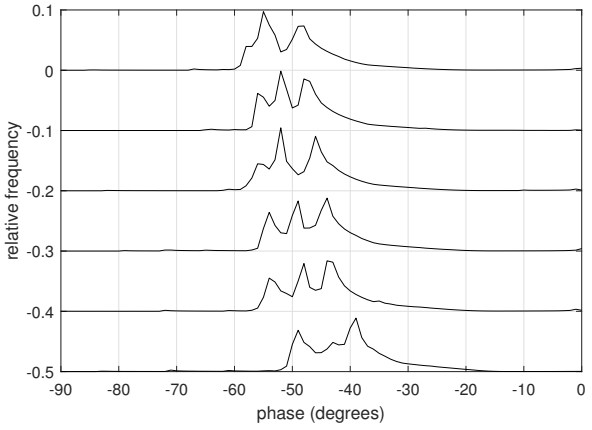

FIGURE 5. The phase between voltage and current as distributed over each of the six sets of cycles, as calculated using Hilbert transforms. The first set is shown in the top trace; the second and subsequent sets are displaced downwards by 0.1 for clarity.

TABLE 4. For each of the six standard cycle sets, we show the cumulative number of times the battery has been cycled by the end of the set, the mean measured efficiency ϵ, the phase difference estimated from the measured efficiency θ_{est}, and the mean measured phase difference from the Hilbert transform, θ_{H}.

Set	Cumulative cycles	$\epsilon(\%)$	ϕ_{est} (rad)	ϕ_{H} (rad)
1	310	87.9(5)	−0.945	−0.837
2	400	87.5(6)	−0.921	−0.816
3	430	87.2(5)	−0.904	−0.794
4	520	86.5(6)	−0.860	−0.771
5	580	86.2(13)	−0.840	−0.754
6	760	84.8(13)	−0.745	−0.681

We note that the measured efficiency drops as the battery ages and as a consequence θ_{est} moves closer to zero. Additionally, the measured phase θ_{H} also moves towards zero. The ratio of the two, $\phi_{\mathrm{est}}/\phi_{\mathrm{H}}$, is roughly constant across the six sets, ranging from 0.87 (for set 5) to 0.91 (for set 6). We do not expect them to be exactly the same since Eq. (15) applies rigorously only for a sine wave stimulus, but nevertheless the two measures are similar. These result also suggest that a move in order of the CPE is responsible for a significant part of the ageing-related drop in efficiency.

C. SYNTHETIC DRIVE PATTERN FOR ELECTRIC CAR

The previous two examples have used simple, repeated current waveforms. For the third situation, we now consider more complicated current waveforms, more akin to the currents that would be experienced by an EV battery, and have used wavelet analysis in order to identify phase differences. An advantage of a complicated waveform is that it contains frequency components across the spectrum and can help distinguish between efficiency changes due to changes in α and those due to changes in R.

1) Experimental method

A synthetic current profile $I(t)$, lasting around three months, was created using the method of Farrow *et al.* [30]. The profile is designed to mimic electric vehicle activity. It shows several hours of constant-current charging (representing a vehicle being charged overnight), followed by a period of a few hours inactivity (when the charging is complete but the vehicle is not in use), then about an hour of charge/discharge activity at high currents (corresponding to a morning commute), then several hours of inactivity followed by about an hour of charge/discharge activity at high currents (corresponding to an evening commute). Randomness is included so that the function is not periodic. A section of the profile is shown in Fig. 6.

Before the profile was applied, the impedance spectrum of an UBCO 3.2 A h 3.6 V 18650 INR $\mathrm{LiNi}_x\mathrm{Mn}_y\mathrm{Co}_{1-x-y}\mathrm{O}_2$ cell was measured using the method of [9]. The synthetic profile was then applied to the cell using a Hewlett Packard 66332A precision current-voltage supply. The actual current applied and the voltage of the battery were monitored continuously. Data were recorded with a sample rate of 8.6 Hz.

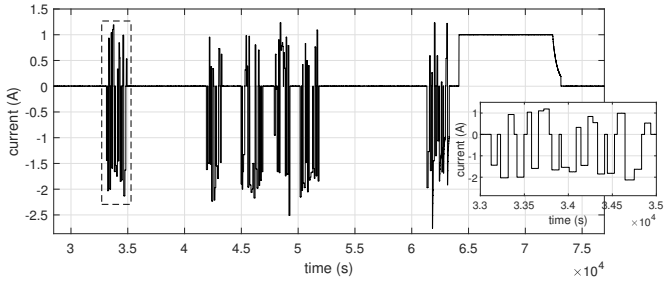

FIGURE 6. A section of the current input to the cell. The inset is a close-up of one of the period of activity indicated by the dashed box.

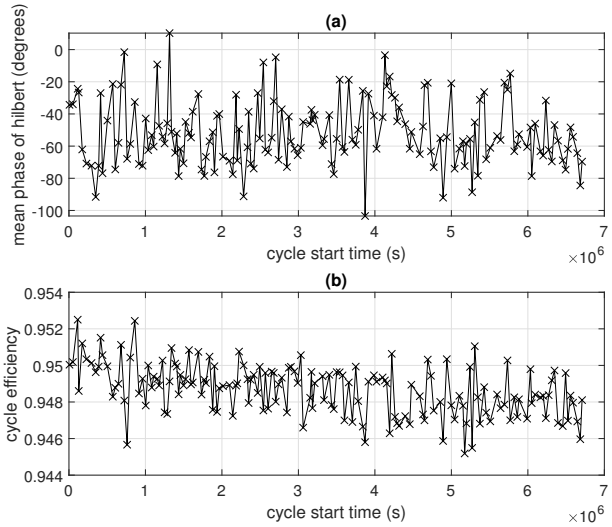

FIGURE 7. (a) The average phase difference between V and I as calculated via a Hilbert Transform (Sec. III-B) over each pseudocycle. (b) The energy efficiency for each pseudocycle.

2) Results

Since the cycles are not periodic, efficiency has been defined over a pseudo-cycle. Specifically, we have identified a pseudo-cycle as starting at a time when the charge (time-integrated current) drops to 50% of its range (*i.e.* is at 50% of the way from its minimum to its maximum), and then ends after it has risen to at least 90% of its range and then dropped again to 50%. Over each pseudo-cycle we have evaluated the energy supplied to the battery E_{in} by integrating $I(t)V(t)$ where I is positive, and evaluated the energy taken out E_{out} by integrating $I(t)V(t)$ where current is negative, and constructing the efficiency $\epsilon = E_{out}/E_{in}$.

Efficiency has been evaluated for each pseudo-cycle. Figure 7(b) shows the efficiency of each successive pseudo-cycle.

3) Analysis

The results of the Hilbert Transform method of Sec. III-B to find the mean phase difference between $V(t)$ and $I(t)$ over a pseudocycle are shown in Fig. 7(a). The results fluctuate considerably because of the many frequency components present

in the signal. This is in contrast to the regular cycling results in Sec. III-B where the periodicity of the cycle is much better defined. The cycle efficiencies also fluctuate considerably for similar reasons, Fig. 7(b), but in this case there is a clear trend to reduced efficiencies as the battery ages, with efficiency ϵ dropping from about 0.950 to 0.948. This is a relative increase in $1-\epsilon$ of 4%.

To proceed we need to use a method appropriate for complicated waveform shapes and for waveforms that are not strictly repeating. We have analyzed the data with a wavelet-based approach, using the Multiscale Oscillatory Dynamics Application (MODA) toolbox produced by Lancaster University github.com/luphysics/moda [25], [26]. The time-series data $V(t)$ and $I(t)$ were split into six equal sections, each 17 days long. To ensure file sizes were sufficiently small for analysis on an Intel i5-1145G7 2.6 GHz processor with 16.0 GB RAM, both $V(t)$ and $I(t)$ were downsampled by a factor 40, to 0.215 Hz. A wavelet transform using a lognorm wavelet was applied to both voltage and current waveforms in each section, to give a spectrogram of voltage $\tilde{V}(f,t)$ and current $\tilde{I}(f,t)$ against both frequency f and time t in that section. Frequency ranges of 10^{-5} Hz to 10^{-3} Hz were initially used, to emphasize the low-frequency region where the CPE impedance is likely to dominate the resistive impedance. Impedances were constructed using $\tilde{Z} = \tilde{V}/\tilde{I}$ (note these are complex quantities) from which an impedance magnitude $|\tilde{Z}(f,t)|$ and phase $\arg[\tilde{Z}(f,t)]$ constructed. The magnitude and phase were both averaged over time t to give a spectrum for magnitude $\hat{Z}(f) = \langle|\tilde{Z}(f,t)|\rangle_t$ and phase $\phi(f) = \langle arg[\tilde{Z}(f,t)]\rangle_t$ for each section. The magnitudes and phases are plotted in Fig. 8. Also shown is the result of the impedance measurement at the start of the experiment. The higher frequency range was also examined — the analysis was repeated but this time for a frequency range of 10^{-3} Hz to 10^{-1} Hz; results are shown in Fig. 9.

First, we note that the impedance spectra reconstructed from the wavelet analysis, in particular day 1–17, are very similar to the impedance spectrum measured directly at the start of the experiment, providing some confidence in the wavelet analysis. Figures 8 shows no obvious differences in the impedance spectra for the 17-day periods considered at frequencies below about 10^{-3} Hz. The variation in $\hat{Z}$ at the very lowest frequencies is likely to be uncertainty due to having only a few periods in the datastream at the lowest frequencies, and is ignored. In the 10^{-5} Hz to 10^{-4} Hz region, the impedance shows CPE-like behaviour, having a constant slope on the $\hat{Z}(f)$ graph and roughly constant phase $\phi(f)$. In contrast to the results of Sec. III-B, there is no indication of a change in phase of the impedance despite Fig. 7(b) showing a small but clear reduction in the energy efficiency. For this particular cell under the conditions tested, the underlying changes responsible for the loss in efficiency with ageing do not appear to be a result of a change in the properties of this CPE.

However, the impedance spectrum at higher frequencies, Fig. 9, shows a clear gain in impedance magnitude as the

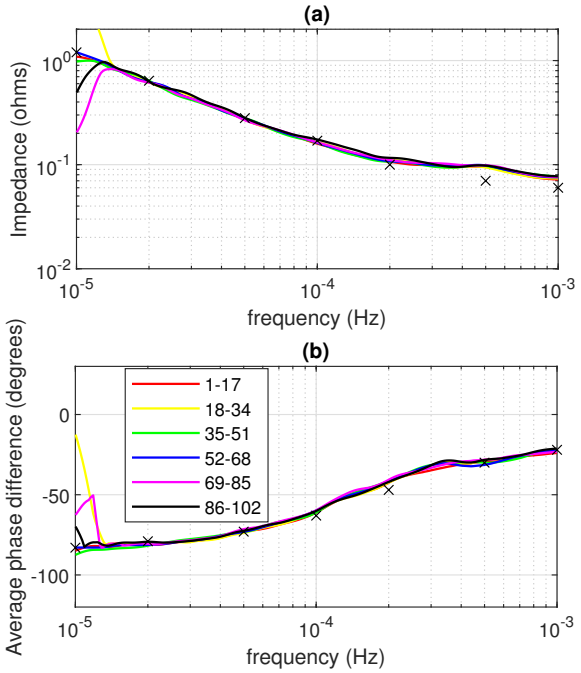

FIGURE 8. (a) The magnitude $\hat{Z}(f)$ and (b) the phase $\phi(f)$ of the wavelet-constructed impedance spectrum at low frequencies, averaged over six seventeen-day sections. The legend shows the start and end day for each section. The black crosses show the results from the impedance measurement at the start of the experiment.

cell ages. At 10^{-1} Hz, the magnitude of impedance rises from about 38.25 mΩ to about 41.00 mΩ from the first and second seventeen-day range to the fifth and sixth, an increase of 2.8% In this spectral region, the impedance is resistor-like as evidenced by the phase difference close to zero. The 2.8% increase in resistance is roughly commensurate with the experimental change in $1-\epsilon$ of about 4% from Fig. 7(b); we would expect the two to be linearly related through Eq. (14).

The implication is that under the tested conditions, this cell demonstrates ageing through increases in its internal resistance R, as opposed to changes in its CPE characteristics.

IV. DISCUSSION

We have used time-series analysis of voltage and current data to probe the changes in batteries as they age. We have assumed that a battery can be described through a CPE-R equivalent circuit model. For the special case of a sine wave stimulation, we have shown theoretically that cycle energy efficiency is related to (i) the order of the CPE, α, which manifests through a phase difference between voltage and current, and (ii) the resistance, R.

The theory has been tested for three cases. In Sec. III-A we have used different charge and discharge currents to cycle a battery, and shown that the order of the CPE element predicted by applying the theory to measured cycle efficiency matches that independently measured through Electrochemical Impedance Spectroscopy.

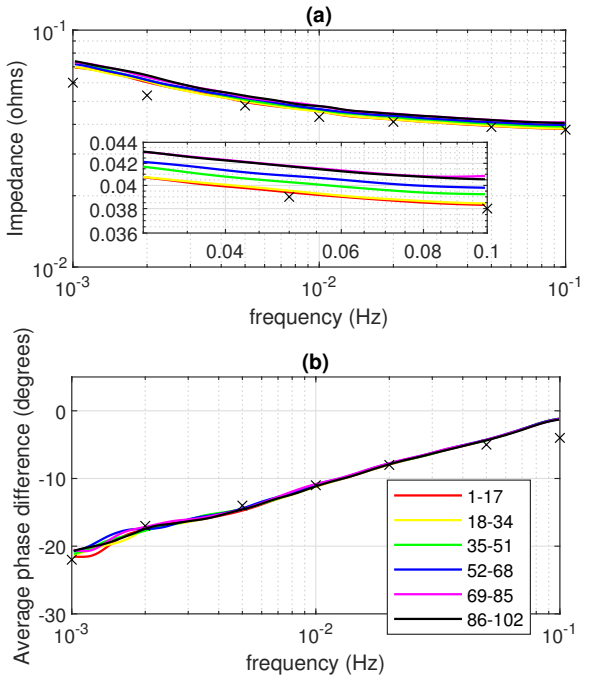

FIGURE 9. **(a) The magnitude $\hat{Z}(f)$ and (b) the phase $\phi(f)$ of the wavelet-constructed impedance spectrum at high frequencies, averaged over six seventeen-day sections. The inset on (a) shows the highest frequencies on a finer scale, indicating a small but discernable rise in impedance magnitude as the battery ages. The legend shows the start and end day for each section. The black crosses show the results from the impedance measurement at the start of the experiment.**

For the case of regular repetitive cycling of a battery in Sec. III-B, the cycle energy efficiency has been measured as the battery ages and the theory applied to predict a move in phase difference towards zero. Analysis of the V and I time-series with Hilbert Transforms have been able to provide another measure of phase difference which is in broad agreement with that predicted from the efficiency measurements, as shown in Table 1.

In the third experiment in Sec. III-C, irregular cycling with a wide range of frequency components has been applied for around 100 days. The analysis in this case is more complicated, since (i) it is difficult to define a cycle, and (ii) the use of a Hilbert Transform is dubious. To identify the change of energy efficiency with ageing, we have needed to use pseudo-cycles — with start and end points being based on returning a battery to a defined state of charge following a significant discharge. This has introduced considerable variation in the results, but cycle energy efficiency still shows a clear downward trend, as shown in Fig. 7(b). For complicated signal patterns, wavelet analysis, for example used to detect disturbances in electrical power systems [29], offers a wave forward. We have used wavelet analysis with V and I time-series to identify changes in phase and impedance with ageing. For the battery tested, the ageing manifests as a rise in impedance at high frequency rather than a change in phase difference.

An implication is that the two batteries, of Secs III-B and III-C, are likely ageing in different ways. While both are reducing in energy cycle efficiency, the underlying mechanisms appear to be different. We emphasize that our theory in Sec. II, and in particular the relationship between cycle energy efficiency and phase of the CPE, Eq. (15), has been derived using only a sine wave stimulus. Our application of it to more complicated signals is therefore not rigorous, but is still insightful. The development of more general theory is mathematically challenging. While we have aimed to keep ambient temperature constant, we finally note that even fluctuations of the size of 1.5°C, which are experienced, may be sufficient to make measurable differences to efficiency and may partly be the cause for the fluctuations in Fig. 7.

V. CONCLUSIONS

By considering phases between voltage and current traces, we have demonstrated that the energy efficiency of a cell relates to the order of a CPE element in its equivalent circuit. In the case of the measured Nickel-Cobalt cell, the drop of efficiency of the cell as it ages can be attributed to a change in the phase difference between voltage and current. Moreover, the analysis has been performed in the time domain, rather than requiring frequency domain measurements such as EIS. The phase-efficiency relationship opens up the possibility of monitoring the state-of-health of a battery from time domain data acquired while a battery is *in situ* in its normal operation.

VI. ACKNOWLEDGMENTS

We thank Aneta Stefanovska and Juliane Bjerkan for valuable discussion regarding the MODA toolbox and wavelet analysis.

REFERENCES

[1] V. Pop, J. B. Henk, D. Danilov, P. P. L. Regtien, and P. H. L. Notten, *Battery Management Systems: Accurate State-of-Charge Indication for Battery-Powered Applications*. Springer, 2008.

[2] M. Huotari, S. Arora, A. Malhi, and K. Främling, "Comparing seven methods for state-of-health time series prediction for the lithium-ion battery packs of forklifts," *Applied Soft Computing*, vol. 111, p. 107670, 2021.

[3] J. A. Osara, O. A. Ezekoye, K. C. Marr, and M. D. Bryant, "A methodology for analyzing aging and performance of lithium-ion batteries: Consistent cycling application," *J. Energy Storage*, vol. 42, p. 103119, Oct. 2021. [Online]. Available: https://linkinghub.elsevier.com/retrieve/pii/S2352152X21008227

[4] C. Pastor-Fernández, T. F. Yu, W. D. Widanage, and J. Marco, "Critical review of non-invasive diagnosis techniques for quantification of degradation modes in lithium-ion batteries," *Renew. Sustain. Energy Rev.*, vol. 109, pp. 138–159, Jul. 2019. [Online]. Available: https://linkinghub.elsevier.com/retrieve/pii/S136403211930200X

[5] C. Hendricks, N. Williard, S. Mathew, and M. Pecht, "A failure modes, mechanisms, and effects analysis (FMMEA) of lithium-ion batteries," *J. Power Sources*, vol. 297, pp. 113–120, Nov. 2015. [Online]. Available: https://linkinghub.elsevier.com/retrieve/pii/S0378775315301233

[6] Y. Fu, J. Xu, M. Shi, and X. Mei, "A fast impedance calculation-based battery state-of-health estimation method," *IEEE Transactions on Industrial Electronics*, vol. 69, no. 7, pp. 7019–7028, 2022.

[7] T. Murariu and C. Morari, "Time-dependent analysis of the state-of-health for lead-acid batteries: An EIS study," *Journal of Energy Storage*, vol. 21, pp. 87–93, 2019. [Online]. Available: https://www.sciencedirect.com/science/article/pii/S2352152X18303712

[8] V. Farrow, "Characterisation of rechargeable batteries: addressing fractional ultralow-frequency devices," Master of Engineering, University of Waikato, Hamilton, New Zealand, Sep. 2020.

[9] C. Dunn, J. B. Scott, and V. Farrow, "A multitone current sink for measuring impedance of in-use batteries," University of Waikato, Report, 2019. [Online]. Available: https://hdl.handle.net/10289/13149

[10] E. Locorotondo, V. Cultrera, L. Pugi, L. Berzi, M. Pierini, and G. Lutzemberger, "Development of a battery real-time state of health diagnosis based on fast impedance measurements," *J. Energy Storage*, vol. 38, p. 102566, 2021.

[11] E. Poihipi, J. Scott, and C. Dunn, "Distinguishability of Battery Equivalent-Circuit Models Containing CPEs: Updating the Work of Berthier, Diard, & Michel," *J. Electroanal. Chem.*, vol. 911, p. 116201, Apr. 2022. [Online]. Available: https://linkinghub.elsevier.com/retrieve/pii/S157266572200193X

[12] U. Westerhoff, K. Kurbach, F. Lienesch, and M. Kurrat, "Analysis of Lithium-Ion Battery Models Based on Electrochemical Impedance Spectroscopy," *Energy Technol.*, vol. 4, no. 12, pp. 1620–1630, 2016.

[13] F. Berthier, J.-P. Diard, and R. Michel, "Distinguishability of equivalent circuits containing CPEs: Part I. Theoretical part," *J. Electroanal. Chem.*, vol. 510, no. 1, pp. 1–11, 2001.

[14] P. Mauracher and E. Karden, "Dynamic modelling of lead/acid batteries using impedance spectroscopy for parameter identification," *J. Power Sources*, vol. 67, no. 1-2, pp. 69–84, 1997.

[15] M. Messing, T. Shoa, and S. Habibi, "Estimating battery state of health using electrochemical impedance spectroscopy and the relaxation effect," *Journal of Energy Storage*, vol. 43, p. 103210, 2021. [Online]. Available: https://www.sciencedirect.com/science/article/pii/S2352152X21009087

[16] O. I. M. Stefan G. Samko, Anatoly A. Kilbas, *Fractional Integrals and Derivatives: Theory and Applications*, 1st ed. CRC Press, 1993.

[17] M. Fouda, A. Elwakil, A. Radwan, and A. Allagui, "Power and energy analysis of fractional-order electrical energy storage devices," *Energy*, vol. 111, pp. 785–792, 2016. [Online]. Available: https://www.sciencedirect.com/science/article/pii/S036054421630723X

[18] J. E. B. Randles, "Kinetics of rapid electrode reactions," *Discuss. Faraday Soc.*, vol. 1, p. 11, 1947.

[19] T. J. Freeborn, B. Maundy, and A. S. Elwakil, "Fractional-order models of supercapacitors, batteries and fuel cells: a survey," *Mater. Renew. Sustain. Energy*, vol. 4, no. 3, p. 9, Sep. 2015.

[20] C. Dunn and J. Scott, "Achieving Reliable and Repeatable Electrochemical Impedance Spectroscopy of Rechargeable Batteries at Extra-Low Frequencies," *IEEE Trans. Instrum. Meas.*, vol. 71, pp. 1–8, 2022. [Online]. Available: https://ieeexplore.ieee.org/document/9789195/

[21] R. Hasan and J. Scott, "Extending Randles's Battery Model to Predict Impedance, Charge–Voltage, and Runtime Characteristics," *IEEE Access*, vol. 8, pp. 85 321–85 328, 2020.

[22] J. Scott and R. Hasan, "New Results for Battery Impedance at Very Low Frequencies," *IEEE Access*, vol. 7, pp. 106 925–106 930, 2019.

[23] T. T. Hartley, J.-C. Trigeassou, C. F. Lorenzo, and N. Maamri, "Energy Storage and Loss in Fractional-Order Systems," *J. Comput. Nonlinear Dyn.*, vol. 10, no. 6, p. 061006, 2015.

[24] T. T. Hartley, R. J. Veillette, J. L. Adams, and C. F. Lorenzo, "Energy storage and loss in fractional-order circuit elements," *IET Circuits Devices Syst.*, vol. 9, no. 3, pp. 227–235, 2015.

[25] P. Clemson, G. Lancaster, and A. Stefanovska, "Reconstructing time-dependent dynamics," *Proceedings of the IEEE*, vol. 104, pp. 223–241, 2016.

[26] P. Clemson and A. Stefanovska, "Discerning non-autonomous dynamics," *Physics Reports*, vol. 542, pp. 297–368, 2014.

[27] M. T. Wilson, C. Dunn, V. Farrow, M. Mucalo, and J. B. Scott, "Measuring electrical properties of batteries at ultra-long timescales," *NCLSI Measure Journal of Measurement Science*, vol. 15, no. 2, pp. 12–16, 2023.

[28] W. Ehm, H. Göhr, R. Kaus, B. Röseler, and C. A. Schiller, "The evaluation of electrochemical impedance spectra using a modified logarithmic Hilbert transform," *Models in Chemistry*, vol. 137, no. 2–3, pp. 145–157, 2000.

[29] V. Sharma and L. Gidwani, "Recognition of disturbances in hybrid power system interfaced with battery energy storage system using combined features of stockwell transform and hilbert transform," *AIMS Energy*, vol. 7, no. 5, pp. 671–687, 2019.

[30] V. Farrow, J. B. Scott, M. J. Cree, and M. T. Wilson, "Passive, fractional, battery equivalent-circuit model in time and frequency domains part 1: Linear model," *in review with IEEE Access*, 2024.

MARCUS WILSON is a Senior Lecturer in Physics and Chemistry in Te Aka Mātuatua – School of Science at The University of Waikato. He has an Honors degree in Physics and Theoretical Physics from the University of Cambridge (1992) and a Ph.D. in theoretical solid state physics from the University of Bristol (1995). He has worked in numerical modeling of physics processes in industry in the U.K. and in academia in New Zealand, the latter since 2004. His research interests include electric properties and dynamics of the human brain, transcranial magnetic stimulation, and more recently batteries.

CHRISTOPHER DUNN (Student Member, IEEE) received the bachelor's degree from the Portsmouth School of Pharmacy, Portsmouth, U.K., in 1985, the master's degree from the Queen's University of Belfast, Belfast, U.K., in 1993, and the Graduate Diploma in Electronics from The University of Waikato, Hamilton, New Zealand, in 2019, where he is currently pursuing the Ph.D. degree. His background is originally in the pharmaceutical sciences, with past specialization in medicinal chemistry (notably quantitative structure–activity relationships and pharmaceutical analysis), pharmaceutical technology, small-scale and aseptic/sterile manufacturing, and quality assurance. He has also worked in scientific communications and in asset management/inspection and line structure engineering for the power supply industry.

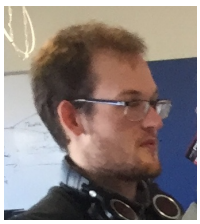

VANCE FARROW obtained 1st class honors in Electronic Engineering at Waikato University in 2018. In 2018 he worked for Nyriad in Cambridge, New Zealand. In 2020 he obtained his ME looking at prediction of battery life using small-signal measurements. He is currently working towards his PhD at Waikato University working on battery management systems using fractional-derivative models and extremely-low frequency electrochemical impedance spectroscopy measurements.

MICHAEL J. CREE (Senior Member, IEEE) received the BSc(Hons) degree in Physics and PhD degree in Electrical and Electronic Engineering from the University of Canterbury in Christchurch, New Zealand in 1990 and 1994, respectively. He is an Associate Professor of Electrical and Electronic Engineering with the University of Waikato, Hamilton, New Zealand. His research interests include medical imaging, computer vision, time-of-flight range imaging, and, more recently, equivalent circuit modeling of batteries.

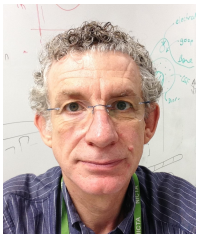

JONATHAN SCOTT (M'80–SM'99) is the Foundation Professor of Electronic Engineering at the University of Waikato, New Zealand. His research interest is characterisation and modeling, particularly applied to implantable electrodes, batteries, semiconductor devices, and acoustic systems. From 1998 to 2006 he was with the Hewlett-Packard and Agilent Technologies Microwave Technology Center in Santa Rosa, California, where he was responsible for advanced measurement systems operating from dc to millimetre-wave. In 1997 and 1998 he was Chief Engineer at RF Technology in Sydney. He was with the University of Sydney in the Department of Electrical Engineering prior to 1997. Professor Scott holds five degrees, has authored over 150 refereed publications, several book chapters and a textbook, and he holds a dozen patents, several covering active products. Professor Scott's educational interests include Threshold Concepts and their application, particularly across engineering disciplines.